

Application of multi-fidelity methods to prediction of gravity currents for uncertainty quantification

By W. Lu[†], A. Ooi[†], L. Thomas, T. Zahtila AND G. Iaccarino

A multi-fidelity strategy has been proposed for approximating the propagation of a lock-exchange gravity current. This involves sampling a low-fidelity (LF) model formulated from shallow-water equations, which is then corrected using interpolative decomposition by high-fidelity direct numerical simulation (DNS) data. We consider applying the bi-fidelity (BF) approximation to a gravity current in a power-law-distributed ambient with three ensemble parameters: stratification strength, ambient height and profile shape. Excellent agreement is found between BF results and DNS provided no interaction, or overrun, occurs between internal waves forming in the ambient and the current front. Attempts to correct for overrun within the LF model are also presented. The time when overrun occurs was found to be sensitive to errors in internal wave and current front velocities. Work is ongoing to further correct for this effect.

1. Introduction

Gravity currents (GCs) are a class of flows that form when a heavy fluid is driven in a lighter ambient by buoyancy, for example, the deposition of a saline solution into fresh water or the release of heavy smoke from wildfires into the atmosphere. Such flows are commonly studied using the lock-exchange problem, where the heavy fluid is suspended by an impermeable barrier, which is then removed, inducing flow.

Propagation of a GC typically follows a number of phases (Maxworthy *et al.* 2002). Initially, the GC accelerates before transitioning into the inertial regime. The first part of which is the slumping phase, where the current propagates at a constant velocity, and the second is the self-similar regime. Finally, once dissipation is dominant, the GC transitions into the viscous phase. Due to the spatially developing nature of a GC, large experimental apparatus or long computational domains are required to resolve propagation, thus resulting in expensive data acquisition. As such, parametric studies have often only employed variation of a small number of effects.

Given the difficulty of obtaining high-fidelity (HF) data, to study interactions between parameters, different approaches are necessary to efficiently sample over the parameter space. Multi-fidelity (MF) methods enable this through a combination of a low-fidelity (LF) model that captures a sufficient amount of the physics for sampling, with corrections being made using accurate HF data. Numerous approaches based on multi-level Monte-Carlo (Fairbanks *et al.* 2017), additive and multiplicative correction (Wenig *et al.* 2023) and interpolative decomposition (ID) (Fairbanks *et al.* 2020) have shown accurate prediction of HF quantities of interest (QoIs) at relatively low cost.

To maintain correlations between the LF and HF models, grid coarsening is typically considered as an LF model. However, such a method only reduces cost by a relatively small amount, given equations of motion are solved. Instead, additional savings may be

[†] Department of Mechanical Engineering, University of Melbourne, Australia

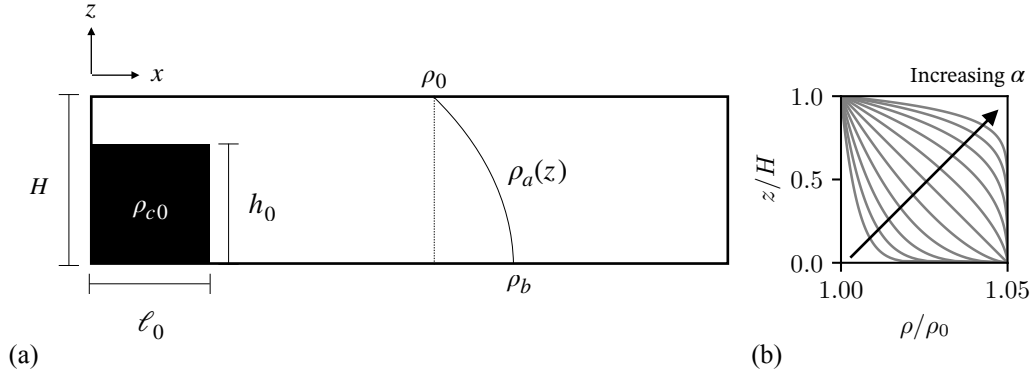


FIGURE 1. (a) Schematic diagram of the lock-exchange problem considered in the present study and (b) variation of ambient density profiles with shape parameter α .

gained through use of low-order models. For GCs, shallow-water equations (SWEs) are a well-studied method to predict propagation (Ungarish & Huppert 2002). Solution of the SWEs is orders of magnitude cheaper than direct numerical simulations (DNSs). Hence, in this report, we construct a MF model utilizing SWEs as an LF model and DNS as a HF model. Analysis of computational cost will also be considered showing the efficiency of the present model compared with Monte-Carlo sampling.

2. Problem formulation

Within this work, the standard planar lock-exchange problem is considered (Figure 1), where a heavy fluid of dimension $h_0 \times \ell_0$ and density ρ_c is placed within an ambient of height H with variable density ranging from ρ_0 at the top boundary to ρ_b at the bottom wall. The ambient density is assumed to vary following the power law

$$\rho_a(z) = \rho_0 \left[1 + \epsilon S \left(1 - \left(\frac{z}{H} \right)^\alpha \right) \right]. \quad (2.1)$$

Here, ρ_0 is the reference density at the top of the ambient, ϵ is a measure of the size of density differences $\epsilon = (\rho_{c0} - \rho_0)/\rho_0$, $S = (\rho_b - \rho_0)/(\rho_{c0} - \rho_0)$ is the stratification strength, and α defines the shape of the ambient profile. Hence, the ensemble parameter space, which we denote Ω , consists of three ensemble parameters, $\{S, H, \alpha\}$. In this work, this is restricted to $\Omega = \{(S, H, \alpha) \in [0.2, 0.5] \times [1, 2] \times [0.1, 10]\}$, although this choice is completely arbitrary and may change based on the QoIs.

3. Multi-fidelity method

The MF method used in the present work is based on the methodology of Hampton *et al.* (2018) and Fairbanks *et al.* (2020), where LF data are corrected with HF data using ID. We thus refer to it as a bi-fidelity (BF) model and detail its construction below.

3.1. Low-fidelity model

We assess the effect of LF model selection by choosing three models with slightly different characteristics, but based on the SWEs. The derivation of the model has been skipped presently for the sake of brevity; however, we refer the reader to our companion paper (Lu *et al.* 2024) for additional details. Hence, it can be shown the SWEs have the form

Case	S	H	α	E_0	ψ	C_D	A	B	c_L	D
ID04	0.499	1.9924	4.7507	0.078	27	1×10^{-3}	0.35	0.7	0.2833	0.7
ID06	0.4943	1.5353	6.4808	0.078	27	1×10^{-3}	0.35	0.7	0.2273	-0.8
ID11	0.4982	1.8166	5.222	0.078	27	1×10^{-3}	0.35	0.7	0.2638	0.2

TABLE 1. Parameter values used for the SWEs with the internal wave model in Fig. 2.

$$\frac{\partial h}{\partial t} + \frac{\partial}{\partial x}(uh) = E|u|, \quad (3.1a)$$

$$\frac{\partial}{\partial t}(uh) + \frac{\partial}{\partial x} \left[u^2 h + \frac{1}{2} g'(c - S) h^2 + \frac{1}{\alpha + 2} g' S \frac{h^{\alpha+2}}{H^\alpha} \right] = -C_D u|u|, \quad (3.1b)$$

$$\frac{\partial}{\partial t}(hc) + \frac{\partial}{\partial x}(huc) = 0. \quad (3.1c)$$

Here, h , u and c are the solution variables describing the current height, fluid velocity and concentration, $g' = \epsilon g$ is the reduced gravity and C_D the drag coefficient. The entrainment coefficient follows Johnson & Hogg (2013), $E = 0.078/(1 + 27Ri)$, with $Ri = g'ch/u^2$ being the bulk Richardson number.

These equations are supplemented with an empirical formulation describing the propagation of the density discontinuity at the current front. We follow Ungarish & Huppert (2002) in formulating this based on the pressure differential at the current front, yielding

$$u_f = Fr(h_f, H) \sqrt{g' h_f \left[c_f - S \left(1 - \frac{1}{1 + \alpha} \left(\frac{h_f}{H} \right)^\alpha \right) - \Delta p' \right]}. \quad (3.2)$$

The first term within the square brackets describes the pressure difference in the absence of stratification, and the second term corrects for stratification effects. Internal waves that may form due to stratification have been shown to interact with the current front, slowing it down before speeding it up again after the wave passes (Maxworthy *et al.* 2002). See, for example, the DNS data in Figure 2. We term this effect overrun hereinafter, which has been modeled with an additional term $\Delta p' = A \operatorname{sech}^2(B(x - c_L t) + D)$, based on solitary wave theory, in the front condition. The parameter c_L describes the speed of the propagating wave and may be determined using linear theory for a given ambient density profile. However, for brevity we refer the reader to Stastna (2022). As for the other parameters, A and B determine wave amplitude and length, and D is the initial formation time. Presently, these parameters have been determined by fitting with DNS data, using the methodology described in the following section (see cases ID04, ID06 and ID11 in Table 2). Values obtained from fitting in Table 1 show excellent agreement with DNS data in Figure 2. We see A and B are equal for all three cases, while D varies for each case. This behavior is undesirable as it implies a dependency on S , H and α , which would be unknown *a-priori*. Thus, a value of $D = 0.033$ has been chosen by averaging values of D in Table 1.

In the case of the zero entrainment (i.e., when $E = C_D = 0$), Eq. (3.1) reduces to the set of equations solved by Ungarish & Huppert (2002). Presently, we solve the system with an in-house Python code using the Lax–Wendroff method for discretization. A total of 401 grid points were used with a time step of $\Delta t U / \ell_0 = 1 \times 10^{-3}$.

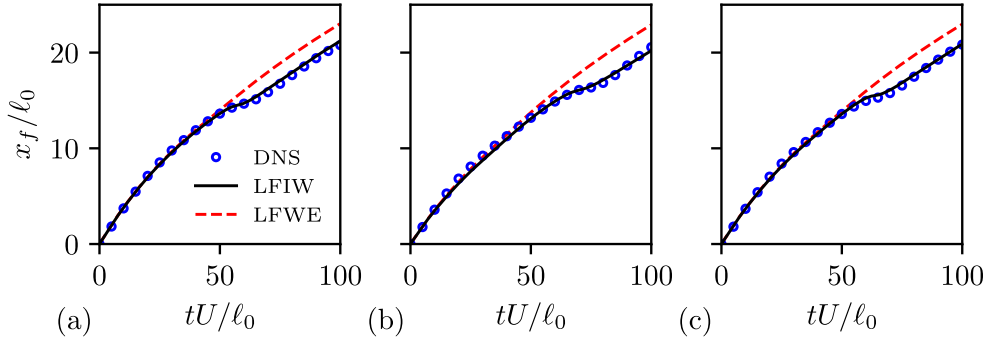


FIGURE 2. Comparison of predictions of front location using the LF model with entrainment (LFWE) and both entrainment and internal wave model (LFIW) with DNS data. Ambient stratification parameters are given by (a) ID04, (b) ID06 and (c) ID11 in Table 1.

3.2. High-fidelity model

For our HF model, we solve the incompressible three-dimensional Navier–Stokes equations with the Boussinesq approximation to model buoyancy effects. To measure the front of the current, we solve an additional advection equation for a passive scalar.

Direct numerical simulations have been conducted using the spectral element solver Nek5000 (Fischer *et al.* 2008). In the spectral element method, primitive variables are projected onto a polynomial basis of compact support on each macro-element. Within each macro-element, function values are represented at the Gauss–Lobatto–Legendre points of order N . The computational domain consists of a box mesh of size $L_x \times L_y \times L_z = 50h_0 \times Hh_0 \times \pi h_0$. In all cases, $E_x = 900$ macro-elements were used in the streamwise direction, and $E_y = 15$ in the span. The number in the wall-normal direction E_z is given in Table 2, leading to a total number E_t of macro-elements ranging between 270,000 and 459,000, in conjunction with a polynomial order of $N = 9$ resulting in meshes with up to 336 million grid points. A buoyancy Reynolds number $Re_b = U\ell_0/\nu$, where $U = \sqrt{g'h_0}$ and ν the kinematic viscosity, of $Re_b = 14,142$ was considered presently. Mesh convergence was assessed using the criteria of Zahtila *et al.* (2023), where local mesh length scales are compared with the Kolmogorov length scale η .

3.3. Bi-fidelity approximation

To construct the BF model, $n = 10,000$ realizations of the LF model have been sampled uniformly random from Ω . The QoIs are then stacked column-wise and placed into an $m \times n$ data matrix \mathbf{A}_{LF} , where each column denotes a different realization in the ensemble. ID is then applied to \mathbf{A}_{LF} to form the decomposition

$$\mathbf{A}_{LF} = \mathbf{B}_{LF}\mathbf{P}, \quad (3.3)$$

where \mathbf{B}_{LF} is an $m \times r$ reduced basis of rank r , which consists of columns of \mathbf{A}_{LF} , and \mathbf{P} is an $r \times n$ weight matrix that reconstructs the other columns from a linear combination of columns in \mathbf{B}_{LF} . The computation of Eq. (3.3) is typically done with a column-pivoted QR decomposition. Assuming \mathbf{P} remains invariant across fidelities, we may replace \mathbf{B}_{LF} with HF data at coinciding parameter values, yielding the BF approximation

$$\mathbf{A}_{BF} = \mathbf{B}_{HF}\mathbf{P}. \quad (3.4)$$

Case	S	H	α	E_z	E_t	N	Grid points
ID00	0.2066	1.9593	0.1648	33	445,500	9	325.9×10^6
ID01	0.4962	1.0012	8.7738	20	270,000	9	197.95×10^6
ID02	0.218	1.0111	0.1215	20	270,000	9	197.95×10^6
ID03	0.4967	1.5088	0.558	27	364,500	9	266.85×10^6
ID04	0.499	1.9924	4.7507	34	459,000	9	335.75×10^6
ID05	0.2343	1.4428	0.1168	27	364,500	9	266.85×10^6
ID06	0.4943	1.5353	6.4808	28	378,000	9	276.69×10^6
ID07	0.2662	1.5162	4.7082	28	378,000	9	276.69×10^6
ID08	0.3327	1.999	8.4456	34	459,000	9	335.75×10^6
ID09	0.4995	1.1376	9.9793	22	297,000	9	217.63×10^6
ID10	0.4993	1.0064	1.5545	20	270,000	9	197.95×10^6
ID11	0.4982	1.8166	5.222	32	432,000	9	316.06×10^6
DNS00	0.4747	1.8491	1.9495	31	418,500	9	306.22×10^6
DNS01	0.3029	1.4347	8.8105	27	364,500	9	266.85×10^6
DNS02	0.243	1.3074	5.5969	25	337,500	9	247.16×10^6
DNS03	0.3609	1.005	5.7965	20	270,000	9	197.95×10^6

TABLE 2. Details of HF cases considered presently along with mesh parameters. Cases with the prefix “ID” are those selected by the interpolative decomposition, and those with “DNS” are those randomly selected in the ensemble.

Presently, HF data is considered at $Re_b = 14,142$. Analysis also conducted for $Re_b = 5,000$ showed similar results and is not presented for brevity.

To assess accuracy of the BF model when incorporating different effects into the LF model, three separate cases were considered with which to test an LF model: no entrainment (LFNE), entrainment (LFWE) and entrainment plus internal wave interaction (LFIW). Parameter values for these models are given in Table 3. Selection of ensemble members in \mathbf{B}_{LF} was made with LFWE using the ID package in SciPy (Virtanen *et al.* 2020). The optimal rank r is typically chosen by evaluating the decay of singular values of \mathbf{A}_{LF} (Fairbanks *et al.* 2020). We plot in Figure 3(a) the singular values for all three LF models. For LFNE and LFWE, the singular values are observed to decay quite rapidly for $k \leq 12$, given by the dashed line, before decaying more slowly for larger k . For LFIW, the decay is slightly slower before a noticeable change in decay rate at $k = 19$.

To ensure the same ensemble members are chosen for reconstruction, the decomposition Eq. (3.3) may involve any submatrix of \mathbf{A}_{LF} . Consider the identity

$$\mathbf{A} = \mathbf{A}\mathbf{A}^+\mathbf{A}, \quad (3.5)$$

where the $^+$ denotes the Moore–Penrose pseudoinverse. The quantity $\mathbf{A}\mathbf{A}^+$ is an identity mapping for the columns of \mathbf{A} , although it need not be an identity matrix. Consider now $\hat{\mathbf{A}}$, a submatrix consisting of s columns of \mathbf{A} , then we may make the approximation

$$\mathbf{A}^r \approx \hat{\mathbf{A}}(\hat{\mathbf{A}}^+\mathbf{A}), \quad (3.6)$$

which is of similar form to Eq. (3.3). Letting $\mathbf{P} = \hat{\mathbf{A}}^+\mathbf{A}$ be the weight matrix yields an equivalent form of Eq. (3.3). Using the ensemble members selected by ID for LFWE, we apply Eq. (3.6) to obtain \mathbf{P} for each LF model.

A second assessment of an appropriate reconstruction rank may also be determined by looking at the total reconstruction error $e = \|\mathbf{A}_{LF}^r - \mathbf{A}_{LF}\|$. In Figure 3(b), we plot e as a function of rank. For LFNE and LFWE, a reduction in error of two orders of magnitude is observed up to $k = 12$, whereas only a single order of magnitude decline is observed increasing k up to 30. By contrast, for LFIW, the error is generally larger for

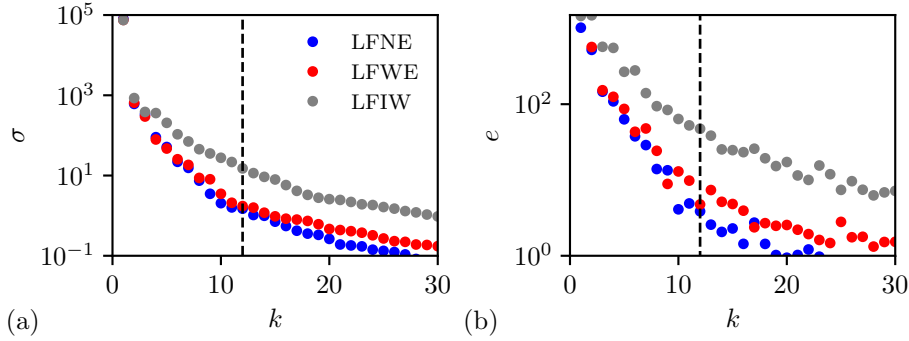


FIGURE 3. (a) Decay of singular values σ and (b) error of LF reconstruction e with reconstruction rank. Dashed lines demarcate the rank of $k = 12$.

BF model	r	LF model	E_0	ψ	C_D	A	B	D
BFNE	12	LFNE	0	—	0	0	—	—
BFWE	12	LFWE	0.078	27	1×10^{-3}	0	—	—
BFIW	12	LFIW	0.078	27	1×10^{-3}	0.35	0.7	0.033

TABLE 3. Details of BF models considered, including LF model parameter values used.

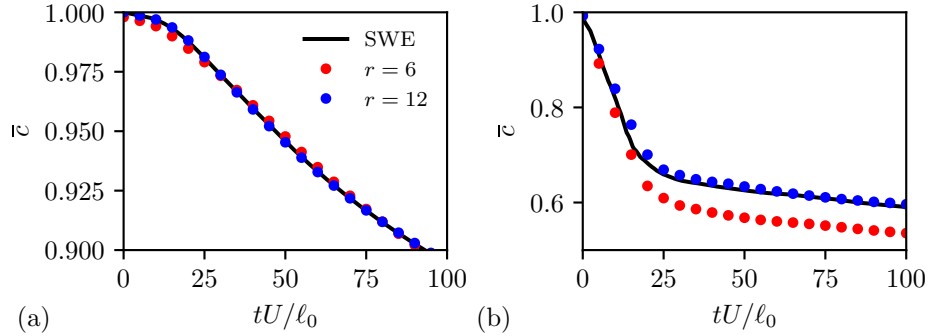


FIGURE 4. Comparison of reconstructed (a) LF data and (b) BF data for ranks of $r = 6$ and $r = 12$ at ensemble parameters corresponding to DNS00.

a given rank and decays slower. However, we also observe a stronger decay for $k \leq 12$ compared with $k > 12$. As e is computed over all matrix elements, large values of e may still show accurate reconstructions. Figure 4(a) shows reconstructed values of mean concentration \bar{c} for ranks of $r = 6$ and 12 at ensemble parameter values corresponding to case DNS00. Good agreement is observed for both ranks, but we note that $r = 6$ shows larger deviations from the SWEs than $r = 12$. Comparison of reconstruction rank for the BF model is also provided in Figure 4(b) for \bar{c} . Two ranks are considered: $r = 6$ and 12. Figure 4(b) shows that using $r = 6$ underpredicts \bar{c} , while $r = 12$ accurately predicts the DNS data. Thus, a reconstruction rank of $r = 12$ has been chosen for the remainder of this study.

3.4. Computational costs

We conclude this section by briefly mentioning the computational costs for obtaining statistical information through a BF strategy compared with utilizing only HF sampling. In the present study, our aim was to obtain 10,000 samples within the chosen parameter space. At approximately 30 seconds per evaluation of the LF model, the matrix \mathbf{A}_{LF} required 83 CPU hours to construct. For the formulation of the BF model, we assume the time taken to compute the ID is negligible (in reality, this was on the order of minutes) compared with the simulation time required for the HF model, which amounted to approximately 4.5 million CPU hours in total for 12 DNSs. Hence, approximately 4.5 million CPU hours are required to construct the BF model. Scaling this up to 10,000 simulations if a Monte-Carlo method is used, approximately 3.8 billion CPU hours would be required to evaluate the HF model 10,000 times, resulting in a cost savings of approximately 800x.

4. Results

To assess the quality of reconstructed variables, we present in this section comparisons of each BF model with DNS results at congruent ensemble parameter values. Four additional HF simulations have been computed at randomly chosen points within the ensemble, which are given in Table 2 by the ‘‘DNS’’ prefix. We consider three QoIs in this section: the current front location x_f , current area A , and mean concentration \bar{c} . We refer to mean concentration here as the concentration averaged over the entire current. In the LF model, x_f is an implicit solution variable, while A and \bar{c} are determined through averaging h and c over the domain. For DNS, an additional passive scalar C is solved with the initial heavy fluid. Measurement of x_f relies on integration of C in the wall-normal direction and determining the point that first exceeds a small threshold above the ambient value (Zahtila *et al.* 2024). Meanwhile, for A and \bar{c} , a boundary separating current and ambient are arbitrarily chosen using a contour of C slightly above the ambient value; a value of 10% density difference has been chosen presently. A is then defined as the area enclosed by this contour, while \bar{c} is the spatially averaged concentration. We plot in Figure 5 comparisons of the BF approximated QoIs (solid lines) with the DNS results (circles) and LF data (dashed lines) at these ensemble parameter values.

Beginning with x_f in Figure 5(*a, d, g, j*), we see the LF data estimate x_f quite well, but typically provide an overestimate for large times, except for LFIW in Figure 5(*a*), where an internal wave forms. In this case, the LFIW model performs quite poorly, estimating the overrun point much earlier than in the DNS. This effect appears to carry over in the BF results, with the overrun occurring at $tU/\ell_0 \approx 30$ for the BFIW results compared with $tU/\ell_0 \approx 60$ in the DNS. For BFNE and BFWE, we find the slight overestimation of x_f is corrected by the BF models, with excellent agreement observed with DNS data aside from when an internal wave forms and interacts with the current front.

Moving onto A [Figure 5(*b, e, h, k*)] and \bar{c} [Figure 5(*c, f, i, l*)], LF results are generally quite poor, significantly underestimating increases in A and decreases in \bar{c} . As expected, the LFNE model predicts constant values of $A/A_0 = 1$ and $\bar{c} = 1$ due to neglecting entrainment in the model. For LFWE and LFIW, increases in A occur due to entrainment being included. Similar observations are also made with \bar{c} , with LFWE and LFIW showing decreases over time. However, the performance of the BF model is more promising for these QoIs than x_f . We find with BFWE, and surprisingly for BFNE, the approximated time series show excellent agreement with DNS results. The ability of BFNE to predict

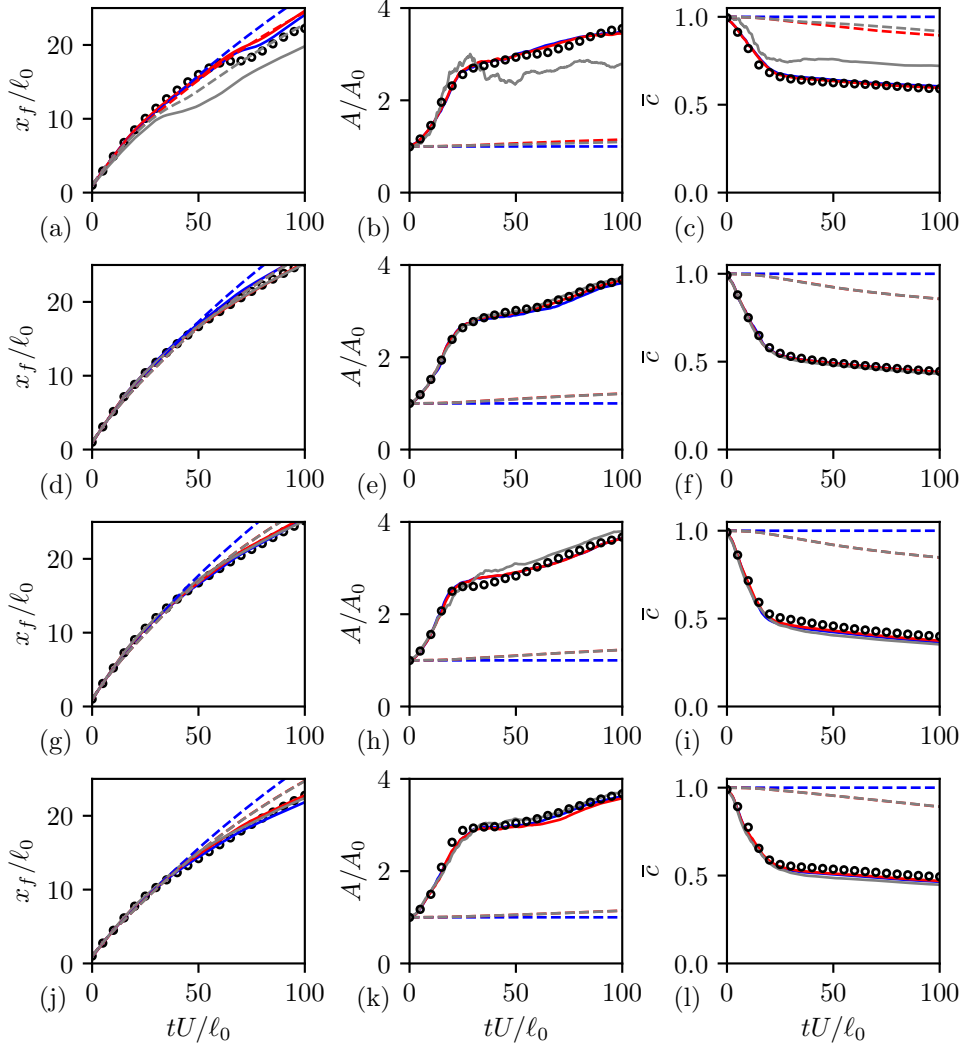


FIGURE 5. Predictions of the front location for the LF model with entrainment (LFWE) and both entrainment and internal wave model (LFIW) with DNS data. Comparisons have been made for ensemble parameter values (a,b,c) DNS00, (d,e,f) DNS01, (g,h,i) DNS02 and (j,k,l) DNS03. Columns correspond to (a,d,g,j) front location, (b,e,h,k) current area and (c,f,i,l) mean concentration.

these QoIs despite entrainment being neglected in the LF Model suggests the correlations in x_f carry over, which we discuss in the following section. Finally, for BFIW, in cases where no interaction occurs between the current front and an internal wave, the approximated values excellently reproduce the DNS data. However, when this interaction occurs, the approximation is a poor representation of DNS values.

5. Discussion

The previous section found the BF model was generally able to accurately correct predictions of the three QoIs considered presently. However, several interesting observations were made, which we further discuss in this section.

The first observation was for the LFNE model, where accurate predictions of the growth in A and decrease in \bar{c} were made despite a lack of entrainment in the LF model. This seemed to indicate that the correlations in x_f are sufficiently accurate to capture the other QoIs despite being disregarded in the LF model. To motivate how this occurs, consider a decomposed data matrix $\mathbf{A} = \mathbf{B}\mathbf{P}$, where QoIs have been stacked on top of one another such that $\mathbf{Q} = [\mathbf{Q}_1^T \cdots \mathbf{Q}_m^T]^T$. As matrix multiplication is conducted row by column, we may consider the top submatrix, x_f presently, giving the equality $\mathbf{A}_1 = \mathbf{B}_1\mathbf{P}$. Now consider the second QoI stacked in \mathbf{A} , which we denote with a subscript 2. We assume both QoIs have the same correlations such that $\mathbf{A}_2 \approx \mathbf{T}\mathbf{A}_1$, with the error given by a small matrix \mathbf{E} . Mathematically stated, we have the affine transformation $\mathbf{A}_2 = \mathbf{T}\mathbf{A}_1 + \mathbf{E}$, hence

$$\mathbf{A}_2 = \mathbf{T}\mathbf{B}_1\mathbf{P} + \mathbf{E}, \quad (5.1a)$$

$$= \mathbf{B}_2\mathbf{P} + \mathbf{E}, \quad (5.1b)$$

$$\approx \mathbf{B}_2\mathbf{P}. \quad (5.1c)$$

Here, $\mathbf{B}_2 \approx \mathbf{T}\mathbf{B}_1$ are the basis vectors of the second QoI, implying that if the correlation is accurately represented linearly between both QoIs, then the reconstruction will be accurate up to the error \mathbf{E} .

In the context of the present case, the GC is physically driven by density differences. As the QoIs considered presently represent global phenomena, we expect trends to be quite similar between the QoIs. For example, increases in stratification have been shown to slow down the evolution of x_f due to the smaller buoyancy force (Zahtila *et al.* 2024). Similarly, smaller density differences with increasing stratification also imply the entrained fluid is heavier, increasing \bar{c} . These results suggest that further cost savings may be made provided one has confidence in QoIs sharing correlations, which is likely when variations in QoIs are driven by the same forces.

The second observation is that despite the LFIW model being able to capture the overrun effect on x_f , Figure 5(a) shows no improvement in the BF model. This suggests that the correlations in the LF model are not representative of those in the HF model, likely based on the constant value of D used in Eq. (3.2). We compare in Figure 6 the measured internal wave speed c_{IW} (blue line) with linear theory predictions c_L (black dashed line) for cases ID04, ID06 and ID11, where internal waves were observed to occur. Fluctuations in the DNS velocity are observed in the early time; thus, we have also plotted a cumulative average $S[c_{IW}]$ (red line). We find c_L approximates the DNS data quite well and captures the changes in wave velocity for different ambient density profiles. It is important to note the relative velocity between the internal wave and the current front dictates the time overrun occurs. Since these velocities are typically of similar magnitude, small errors in both c_L used for the LF model and the front velocity u_f will result in large discrepancies for the overrun time. As a result, correlations present in the LF model are not representative of those in its HF counterpart, hence providing a poor base to construct the BF model, leading to inaccurate predictions when overrun is present [Fig. 5(a, b, c)]. We also remark this effect explains the varying values of D (Table 1) required to capture the overrun location in Figure 2. Our observations, not shown presently, found

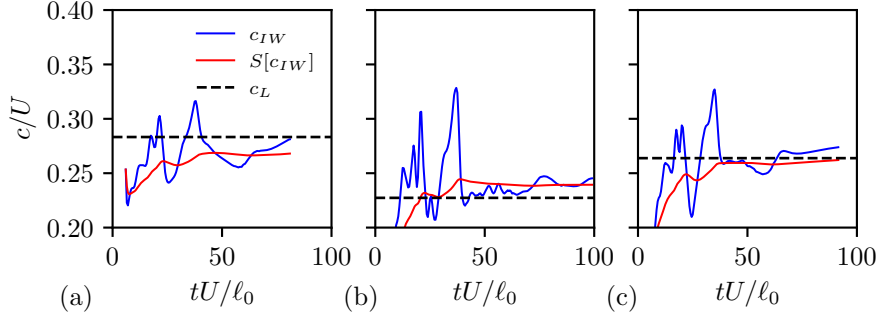


FIGURE 6. Comparison of internal wave velocity predicted by linear theory with DNS data. Ambient stratification parameters are given by (a) ID04, (b) ID06 and (c) ID11 in Table 1.

the internal wave formation time for cases ID04, ID06 and ID11 to be constant, implying a constant D . Therefore, discrepancies in c_L and u_f will inaccurately predict the relative velocity, requiring changes in D to compensate.

6. Conclusions and outlook

This report proposes a BF strategy for prediction of GC statistics. An LF model based on the SWEs is first used to sample within a chosen parameter space. Then, ID is applied to the formed data matrix to determine appropriate ensemble parameter values for reconstruction. HF data at said values are finally used to form the BF approximation, enabling for approximately 800x computational cost savings.

The BF strategy has been applied to a lock-exchange GC with a power-law-distributed ambient density, defined by three ensemble parameters: stratification strength, ambient height and profile shape. Three BF models based on the SWEs with (BFWE) and without (BFNE) entrainment, along with entrainment plus an internal wave model (BFIW), were considered. BF models BFWE and BFNE, despite its lack of entrainment, were shown to approximate DNS data extremely well except when an internal wave interacted with the current front. It was determined this accuracy in BFNE was a consequence of correlations in x_f carrying over to A/A_0 and \bar{c} . Meanwhile, attempts to model this effect in the LF model resulted in poor BF approximations. This is likely due to small errors in both c_L and u_f causing large errors in the relative velocity, thereby resulting in large errors in overrun time.

While not detailed in the present report, ongoing work utilizing the BF model for uncertainty quantification is being conducted. Sensitivity of QoIs to ensemble parameters is an important aspect of understanding uncertainty propagation and physical processes in the model and will be explored further in future work.

Acknowledgments

We thank E. Meiburg, A. Leonelli and S. Balachandar for the insightful discussions.

REFERENCES

- FAIRBANKS, H. R., DOOSTAN, A., KETELSEN, C. & IACCARINO, G. 2017 A low-rank control variate for multilevel Monte Carlo simulation of high-dimensional uncertain systems. *J. Comput. Phys.* **341**, 121–139.

- FAIRBANKS, H. R., JOFRE, L., GERACI, G., IACCARINO, G. & DOOSTAN, A. 2020 Bi-fidelity approximation for uncertainty quantification and sensitivity analysis of irradiated particle-laden turbulence. *J. Comput. Phys.* **402**, 108996.
- FISCHER, P. F., LOTTES, J. W. & KERKEMEIER, S. G. 2008 Nek5000. <https://nek5000.mcs.anl.gov/>.
- HAMPTON, J., FAIRBANKS, H. R., NARAYAN, A. & DOOSTAN, A. 2018 Practical error bounds for a non-intrusive bi-fidelity approach to parametric/stochastic model reduction. *J. Comput. Phys.* **368**, 315–332.
- JOHNSON, C. G. & HOGG, A. J. 2013 Entraining gravity currents. *J. Fluid Mech.* **731**, 477–508.
- LU, W., LAM, W. K., ZAHTILA, T., CHAN, L., SUTHERLAND, D., MOINUDDIN, K., MANASSEH, R., IACCARINO, G. & OOI, A. 2024 Modelling the effects of gravity current propagation in a nonlinearly stratified ambient with shallow-water-type equations. (in preparation)
- MAXWORTHY, T., LEILICH, J., SIMPSON, J. E. & MEIBURG, E. H. 2002 The propagation of a gravity current into a linearly stratified fluid. *J. Fluid Mech.* **453**, 371–394.
- STASTNA, M. 2022 *Internal Waves in the Ocean*. Surveys and Tutorials in the Applied Mathematical Sciences, Vol. 9. Springer International Publishing.
- UNGARISH, M. & HUPPERT, H. E. 2002 On gravity currents propagating at the base of a stratified ambient. *J. Fluid Mech.* **458**, 283–301.
- VIRTANEN, P., GOMMERS, R., OLIPHANT, T. E., HABERLAND, M., REDDY, T., COURNAPEAU, D., BUROVSKI, E., PETERSON, P., WECKESSER, W., BRIGHT, J. 2020 SciPy 1.0: fundamental algorithms for scientific computing in Python. *Nat. Methods.* **17**, 261–272.
- WENIG, P. J., KELM, S. & KLEIN, M. 2023 CFD Uncertainty Quantification using stochastic spectral methods—Exemplary application to a buoyancy-driven mixing process. *Nucl. Eng. Des.* **409**, 112317.
- ZAHTILA, T., LAM, W.K., CHAN, L., SUTHERLAND, D., MOINUDDIN, K., DAI, A., SKVORTSOV, A., MANASSEH, R. & OOI, A. 2024 On the propagation of planar gravity currents into a stratified ambient. *Phys. Fluids* **36**, 036601.
- ZAHTILA, T., LU, W., CHAN, L. & OOI, A. 2023 A systematic study of the grid requirements for a spectral element method solver. *Comput. Fluids* **251**, 105745.